Quantum Optical Simulator for Unruh–DeWitt Detector Dynamics

Tai Hyun Yoon 61,2,*

¹Department of Physics, Korea University, Anam-ro 145, Seongbuk-gu, Seoul 02841, Republic of Korea

²Center for Molecular Spectroscopy and Dynamics, IBS, Anam-ro 145, Seongbuk-gu, Seoul 02841, Republic of Korea

We present a quantum-optical platform for simulating relativistic detector-field interactions using entangled nonlinear biphoton sources (ENBSs), realized through phase-controlled single-photon frequency-comb (SPFC) sources. By mapping the dynamical evolution of this system onto the Unruh–DeWitt (UDW) detector model, we show that signal-mode excitations emulate detector transitions driven by vacuum fluctuations, while coherently seeded idler modes act as an effective quantum field. This correspondence enables tabletop exploration of Unruh-like excitation, coherence harvesting, and field-induced entanglement. We derive the effective interaction Hamiltonian and Lindblad master equation for two coherently seeded ENBS units and obtain analytical solutions for the signal photon number $N_{\text{sig}}(t)$ and second-order correlation function $g^{(2)}(0;t)$. Numerical simulations confirm that phase-dependent biphoton dynamics reproduce UDW-type behavior, including tunable excitation and quantum correlations. The output signal state exhibits controllable fidelity, interference visibility, and entanglement entropy as functions of the seeding phase and amplitude. These results establish ENBSs as experimentally accessible quantum simulators of relativistic field phenomena, providing a photonic testbed for analog gravitational effects, vacuum fluctuations, and spacetime-induced coherence—all within reach of current nonlinear-optics technology.

 $^{^*}$ thyoon@korea.ac.kr

I. INTRODUCTION

The Unruh–DeWitt (UDW) detector model is a foundational concept in relativistic quantum field theory, describing the dynamics of localized two-level systems coupled to quantum fields [1–3]. This model captures profound phenomena such as the Unruh effect and entanglement harvesting—where entanglement between spacelike-separated detectors emerges via local interactions with a shared quantum field [4–13].

In particular, the Unruh effect predicts that a uniformly accelerated observer perceives the Minkowski vacuum as a thermal bath at the Unruh temperature $T_U = \hbar a/(2\pi c k_B)$, where a is the observer's proper acceleration, \hbar is the reduced Planck constant, c is the speed of light, and k_B is the Boltzmann constant [1, 9]. In the UDW framework, this thermality arises from the detector's excitation rate, which is governed by the Wightman function of the quantum field evaluated along the accelerated trajectory [3, 14]. While direct observation of such effects in high-energy physics remains elusive, they have inspired a growing body of analog quantum simulations [13–28].

Among recent breakthroughs, two independent experiments using Bose–Einstein condensates (BECs) have demonstrated analogs of UDW detector dynamics. In one approach, Hu et al. [9] employed a parametrically modulated potential to generate matter-wave radiation with thermal statistics consistent with the Unruh effect, observing long-range coherence and temporal reversal indicative of Unruh-like quantum fluctuations. Separately, Viermann et al. [25] engineered an artificial event horizon within an atomic BEC and measured entanglement between spatially separated quasiparticle excitations, directly simulating the detector–field entanglement structure predicted by the UDW model. While powerful, such atomic platforms rely on many-body interactions and tailored trapping potentials, which constrain their tunability, scalability, and direct integration with photonic quantum technologies.

In this work, we propose a fully photonic and inherently quantum optical analog platform that emulates UDW detector dynamics using entangled nonlinear biphoton sources
(ENBSs) [29, 30]. Our simulator exploits seeded single-photon frequency comb (SPFC)
sources based on periodically-poled lithium niobate (PPLN) crystals, enabling tabletop replication of relativistic detector—field interactions through accessible nonlinear optics. Each
SPFC source is coherently seeded via a narrow-linewidth idler field, and the output signal
photons act as analogs of detector excitations.

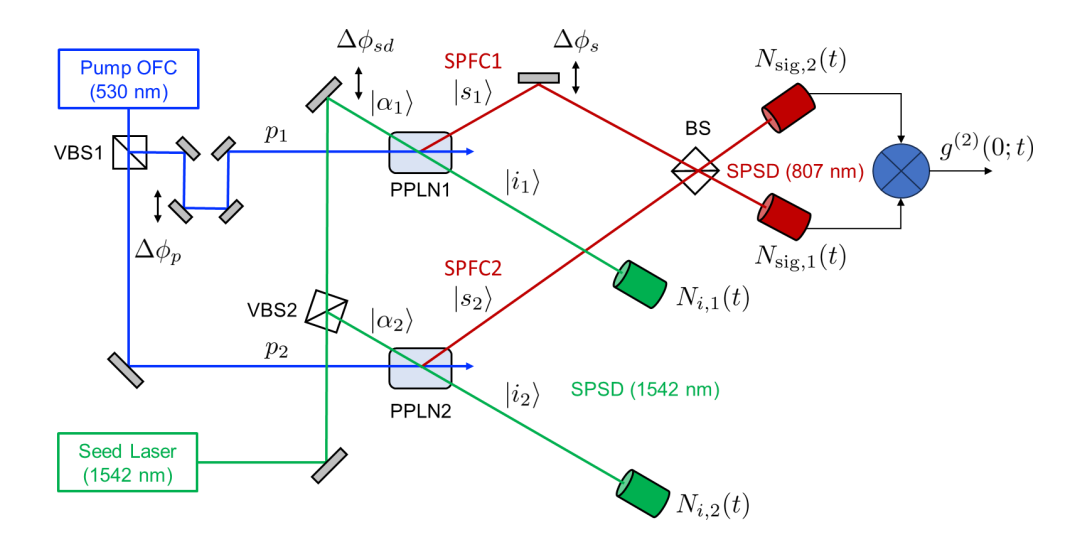


FIG. 1. Quantum-optical analog simulator of Unruh-DeWitt detector dynamics.

Two entangled nonlinear biphoton sources (ENBSs), each realized using a seeded single-photon frequency-comb (SPFC) generator, are implemented with periodically poled lithium niobate (PPLN) crystals pumped by optical frequency combs. Coherent seed fields at 1542 nm with a controllable relative phase $\Delta\phi_{\rm sd}$ are injected into the idler paths. The resulting signal outputs at 807 nm exhibit quantum correlations analogous to Unruh–DeWitt detector excitations mediated by a shared vacuum field. The mean photon number $N_{\rm sig}(t)$ is measured by removing the beam splitter (BS), while the second-order correlation function $g^{(2)}(0;t)$ is obtained via coincidence detection at the two outputs. Alternatively, when a single detector is placed after the combining BS, the setup measures the first-order (single-photon) coherence of the signal field—demonstrating phase-sensitive interference as in Refs. [29, 30]. BS: beam splitter; VBS: variable beam splitter; SPSD: single-photon-sensitive detector.

Figure 1 illustrates the conceptual architecture of the simulator [29, 30]. Two SPFC sources are pumped by optical frequency combs at 530 nm, and their idler channels are seeded with coherent fields α_1 and α_2 at 1542 nm, with tunable relative phase $\Delta\phi_{\rm sd}$. The resulting signal photons at 807 nm exhibit quantum correlations controlled by this phase difference, enabling phase-resolved probing of detector-detector entanglement.

Depending on the detection configuration, the setup can access complementary observables. Removing the combining beam splitter (BS) yields the mean signal photon number $N_{\text{sig}}(t)$; coincidence detection at the BS outputs provides the second-order correlation function $g^{(2)}(0;t)$; and, importantly, monitoring a single output after the BS enables measurement of the single-photon detection rate $R(\Delta\phi_{\rm sd})$, which reveals the first-order (single-photon) coherence of the signal field as a function of the seeding phase difference $\Delta\phi_{\rm sd}$ [29, 30]. This first-order coherence corresponds to interference between excitation amplitudes of the two effective detectors, thereby revealing the phase-sensitive, vacuum-mediated correlations central to the UDW analogy.

Compared to analog gravity experiments using BECs [9, 25], our ENBS-based platform offers several distinct advantages. In the first BEC implementation, Hu et al. demonstrated matter-wave radiation with thermal Unruh-like statistics through time-dependent trapping and parametric modulation. More recently, Viermann et al. engineered an artificial horizon in a BEC and directly observed spatial entanglement between quasiparticles—constituting an experimental realization of detector–field entanglement predicted by the UDW model. While these matter-wave platforms reveal rich many-body analogs of relativistic field theory, they rely on complex collective dynamics and specialized trapping geometries.

In contrast, our quantum optical simulator in Fig. 1 enables coherent, phase-resolved control over entangled single-photon states using well-characterized nonlinear interactions. It integrates naturally with scalable photonic technologies and provides direct access to complementary observables: the time-dependent signal-mode excitation number $N_{\text{sig}}(t)$, the second-order correlation function $g^{(2)}(0;t)$, and the single-photon detection rate $R(\Delta\phi_{\text{sd}})$, which reveals the first-order interference visibility as a function of the seeding phase difference $\Delta\phi_{\text{sd}}$ [29, 30]. These observables together allow quantitative characterization of coherence, fidelity, and entanglement in an experimentally tunable setting, establishing our ENBS architecture as a versatile platform for simulating Unruh–DeWitt detector dynamics and quantum field interactions in flat spacetime.

Unlike metric-based analog platforms that emulate spacetime curvature via effective Rindler transformations, such as those demonstrated in BECs [9, 25], our approach focuses on reproducing the *dynamical response* of UDW detectors to vacuum fluctuations. While the BEC experiments observe thermal radiation consistent with the Unruh effect via modulated trapping potentials and dynamical horizons, they rely on many-body excitations and collective wave dynamics that constrain optical access and scalability. By contrast, our system implements a fully quantum-optical analog using seeded nonlinear biphoton sources, offering a compact, tunable, and phase-resolved simulator of relativistic detector—field interactions.

We derive the Hamiltonian dynamics and Lindblad master equation governing our ENBS architecture, yielding closed-form expressions for key observables: the signal-mode photon number $N_{\text{sig}}(t)$ and the second-order correlation function $g^{(2)}(0;t)$. These quantities depend on a local seeding phase Φ_N and a global interferometric phase Φ , allowing the separation of spontaneous excitation from stimulated amplification. In particular, the condition $\Phi = \pi/2$ leads to strong bunching in $g^{(2)}(0;t)$, indicating biphoton entanglement analogous to vacuum-induced detector correlations.

Our analytical results are supported by numerical simulations using experimentally realistic parameters. The simulations reveal coherent signal amplification followed by saturation due to Lindblad damping, as well as sharp phase-dependent behavior in both gain and bunching. These phenomena are tunable via the coherent seeding amplitudes and phases, highlighting the ENBS platform's capability to simulate both local detector dynamics and nonlocal coherence features of relativistic quantum field theory.

In addition to reproducing excitation dynamics, our model directly encodes quantum information observables into the signal-mode output. By adjusting the seed field amplitudes and relative phase $\Delta\phi_{\rm sd}$, we continuously control the signal-mode fidelity, visibility, and entanglement entropy. These measures are quantitatively derived in Section III C, and follow the exact complementarity relation for wave–particle–entanglement duality [30], enabling tabletop exploration of relativistic information flow.

Compared to circuit QED analogs [31], moving mirrors [32], and recent proposals using modulated superconducting qubits [33, 34] or time-dependent optical lattices [13, 21, 35, 36], our ENBS-based simulator operates at the single-photon level and allows fully optical phase-resolved control of vacuum analog interactions. The observable $g^{(2)}(0;t)$, in particular, offers a direct probe of nonlocal entanglement and field-mediated correlations, paralleling entanglement harvesting in the UDW model.

Although our simulator employs a discrete seeded idler mode rather than a field-theoretic continuum, it faithfully captures the local detector response to structured vacuum-like correlations. The idler field mediates both spontaneous excitation and quantum interference effects, while signal-mode damping introduces physically realistic loss and decoherence—effectively mimicking detector inefficiency and environmental back-action. These features preserve the essential physics of UDW detector dynamics in a highly accessible optical platform.

When two ENBS units share a common idler mode and are coherently seeded, their signal outputs exhibit nonlocal entanglement without direct interaction—realizing a photonic analog of entanglement harvesting from a shared quantum field. This establishes the ENBS architecture as a versatile and scalable framework for simulating relativistic quantum effects, including horizon physics, vacuum entanglement, and causal structure, with potential extensions to spatially separated detector arrays and multi-mode continua.

II. QUANTUM OPTICAL SIMULATOR FRAMEWORK: MODELING UNRUH-DEWITT DYNAMICS

We begin by modeling each spontaneous parametric frequency-conversion process in the ENBS architecture (Fig. 1) using an effective nonlinear interaction Hamiltonian [29]:

$$\hat{H}_{\text{ENBS}} = \hbar |g_{\text{eff}}| \sum_{j=1}^{2} \left(e^{i\phi_{p,j}} \hat{A}_{\text{SM},j}^{\dagger} \hat{a}_{i,j}^{\dagger} + e^{-i\phi_{p,j}} \hat{A}_{\text{SM},j} \hat{a}_{i,j} \right), \tag{1}$$

where $\hat{a}_{i,j}$ annihilates the idler field and $\hat{A}_{\text{SM},j}$ is the signal supermode annihilation operator associated with the j-th ENBS. Each effective coupling constant is written as

$$g_{\text{eff},j} = |g_{\text{eff}}|e^{i\phi_{p,j}},\tag{2}$$

with $\phi_{p,j}$ denoting the phase of the pump driving the j-th crystal. The overall gain magnitude $|g_{\text{eff}}|$ characterizes the nonlinear interaction strength per unit time under undepleted-pump conditions.

The signal supermode operator for the j-th entangled nonlinear biphoton source (ENBS) collects the 2N+1 discrete signal frequency bins that are phase-matched to the optical frequency-comb pump. Under the uniform-coupling approximation $g_n^{(j)} = g_0^{(j)} e^{i\phi_{g_0^{(j)}}}$ (see Supplementary Information (SI) Sec. S1), all bins experience identical gain magnitude and phase, so only one collective signal mode couples effectively to the idler. The corresponding normalized supermode operator is defined as

$$\hat{A}_{\text{SM},j} = \frac{e^{-i\phi_{g_0^{(j)}}}}{\sqrt{2N+1}} \sum_{n=-N}^{N} \hat{a}_{s,n}^{(j)}, \tag{3}$$

which satisfies the canonical commutation relation $[\hat{A}_{\text{SM},j}, \hat{A}_{\text{SM},j}^{\dagger}] = 1$. Here $\hat{a}_{s,n}^{(j)}$ annihilates a signal photon in the *n*-th frequency bin of source *j*. The overall phase factor $e^{-i\phi_{g_0^{(j)}}}$ aligns

TABLE I. Conceptual correspondence between components of the ENBS optical simulator and Unruh–DeWitt (UDW) detector models in relativistic quantum field theory. The ENBS system replicates local excitation, coherence control, and entanglement harvesting via experimentally tunable optical interactions.

Aspect	UDW Detector (Quantum	ENBS Optical Simulator (This
	Field Theory)	Work)
Detector excitation	Two-level system transition op-	Signal-mode photon creation opera-
	erator $\hat{\sigma}_+$	tor $\hat{A}_{\mathrm{SM}}^{\dagger}$
Field reservoir	Scalar quantum field $\hat{\phi}(x)$, con-	Discrete idler mode \hat{a}_i seeded by a
	tinuum modes	coherent field
Detector-field interac-	Local coupling $\hat{\sigma}_+\hat{\phi}(x) + \text{h.c.}$	Nonlinear $\chi^{(2)}$ parametric interac-
tion		tion with coherent pump
Excitation mechanism	Wightman function $G^+(x, x')$ de-	Temporal gain function $N_{\text{sig}}(t)$ un-
	termines excitation rate	der seeded SPFC dynamics
Coherence and phase	Detector trajectory and field cor-	Relative seeding phase $\Delta\phi_{\rm sd},$ pump
control	relations set excitation phase	phases, and amplitude asymmetry
		between α_1, α_2
Quantum observables	Detector response $\langle \hat{\sigma}_+ \hat{\sigma} \rangle$, exci-	$N_{\rm sig}(t), \ g^{(2)}(0;t), \ R(\Delta\phi_{\rm sd}), \ {\rm and}$
	tation probability, decoherence	signal-mode fidelity and visibility
Entanglement harvest-	Nonlocal correlations from vac-	Signal-mode entanglement from in-
ing	uum entangle spacelike detectors	terference of two ENBSs sharing a
		common or correlated idler channel
Mixedness and deco-	Tracing over inaccessible space-	Tracing over idler modes and vac-
herence	time regions (e.g., Rindler	uum contributions in the reduced
	wedge)	signal density matrix

the collective signal mode with the complex coupling constant, ensuring a real, positive effective coupling $G_{\text{eff}} = |g_0^{(j)}| \sqrt{2N+1}$. This single collective supermode interacts with the coherently seeded idler mode according to the effective two-mode Hamiltonian of Eq. (1).

This Hamiltonian captures the essential physics of biphoton generation via parametric down-conversion and serves as a direct analog to the UDW interaction Hamiltonian, where

a localized detector couples to a scalar quantum field. In this mapping, the signal mode represents the detector's excitation degree of freedom, while the idler mode mimics the mediating quantum field (see Table I). The relative pump phase $\Delta \phi_p = \phi_{p,1} - \phi_{p,2}$ and idler-seeding phase $\Delta \phi_{\rm sd} = \phi_{\alpha,1} - \phi_{\alpha,2}$ act as tunable parameters controlling the effective coupling and coherence, enabling quantum simulation of relativistic detector–field dynamics.

Each idler mode is coherently seeded with $\alpha_j = |\alpha| e^{i\phi_{\alpha,j}}$, providing phase control over signal-photon generation. Taking ENBS2 as the reference arm $(\phi_{p,2} = \phi_{s,2} = \phi_{\alpha,2} = 0)$, we define the key local and global phase parameters:

$$\Phi_N \equiv \phi_{p,1} - \phi_{\alpha,1},\tag{4a}$$

$$\Phi \equiv \phi_{p,1} - (\phi_{\alpha,1} + \phi_{s,1}),\tag{4b}$$

where Φ_N characterizes the local pump–seed phase mismatch determining single-source gain, and Φ denotes the global interferometric phase that governs nonlocal correlations between the two signal modes. The seeding-phase difference $\Delta\phi_{\rm sd} = \phi_{\alpha,1} - \phi_{\alpha,2}$ introduced in Fig. 1 is experimentally adjustable and directly determines the single-photon interference pattern $R(\Delta\phi_{\rm sd})$.

The same phase conventions allow us to formulate the single-photon detection rate at one output of the combining beam splitter, $R(\Delta\phi_{\rm sd})$, in terms of first-order coherence of the signal modes. For a balanced beam splitter combining the two signal supermodes, $\hat{A}_{\pm} = (\hat{A}_{\rm SM,1} \pm \hat{A}_{\rm SM,2})/\sqrt{2}$, the count rate at a given output is proportional to the normally ordered expectation value

$$R(\Delta\phi_{\rm sd}) \propto \left\langle \hat{A}_{\rm out}^{\dagger} \hat{A}_{\rm out} \right\rangle = N_{\rm sig,1}(t) + N_{\rm sig,2}(t) + 2 \Re \left[e^{i\Delta\phi_{\rm sd}} \left\langle \hat{A}_{\rm SM,1}^{\dagger} \hat{A}_{\rm SM,2} \right\rangle \right], \tag{5}$$

where $\Delta\phi_{\rm sd}$ denotes the effective seeding-phase difference between the two idler inputs. The sinusoidal modulation of $R(\Delta\phi_{\rm sd})$ provides a direct measure of the first-order interference visibility between the ENBS branches, as demonstrated experimentally in Refs. [29, 30]. In our framework this quantity follows from the same reduced signal-mode density matrix used below to characterize fidelity and coherence, and constitutes the single-detector analog of the UDW response function.

To incorporate realistic decoherence effects in the signal mode, we extend the idealized

unitary dynamics of the ENBS architecture using the Lindblad master equation:

$$\frac{d\hat{\rho}}{dt} = -\frac{i}{\hbar} [\hat{H}_{\text{ENBS}}, \hat{\rho}] + \sum_{j=1}^{2} \left[\mathcal{D}[\sqrt{\kappa_s} \hat{A}_{\text{SM},j}] + \mathcal{D}[\sqrt{\kappa_i} \hat{a}_{i,j}] \right] \hat{\rho}, \tag{6}$$

where $\mathcal{D}[\hat{L}]\hat{\rho} = \hat{L}\hat{\rho}\hat{L}^{\dagger} - \frac{1}{2}\{\hat{L}^{\dagger}\hat{L},\hat{\rho}\}$ is the standard Lindblad dissipator, and κ_s and κ_i denote the decay rates of the signal and idler modes, respectively.

Under the undepleted-pump approximation and assuming initial coherent idler seeding, the analytical solution of the Heisenberg–Langevin equations yields the damped signal photon number from each SPFC unit as

$$N_{\text{sig},j}(t) = \left[1 + |\alpha_j|^2 + 2|\alpha_j|\cos(\Phi_{N,j})\right] \times \sinh^2(|g_{\text{eff}}|t)e^{-\kappa_s t}, \tag{7}$$

where $\Phi_{N,j} = \phi_{p,j} - \phi_{\alpha,j}$ is the local phase difference between the pump and idler seeding fields. In the symmetric case $|\alpha_1| = |\alpha_2| = |\alpha|$ and $\Phi_{N,1} = \Phi_{N,2} = \Phi_N$, giving $N_{\text{sig},j}(t) \equiv N_{\text{sig}}(t)$.

The normalized second-order correlation function at zero delay is then

$$g^{(2)}(0;t) = 1 + F \left[\frac{|\alpha_1|^2 |\alpha_2|^2 \sin^2 \Phi}{N_{\text{sig},1}(t) N_{\text{sig},2}(t)} \right], \tag{8}$$

where $\Phi = \phi_{p,1} - (\phi_{\alpha,1} + \phi_{s,1} - \phi_{s,2})$ is the global phase difference accumulated across the interferometer, and F is the conditional fidelity between the idler branches,

$$F = |\langle \alpha_1, 1 | \langle \alpha_2 | \alpha_1 \rangle | \alpha_2, 1 \rangle|, \qquad (9)$$

quantifying the overlap between the entangled biphoton modes emitted by the two SPFC sources (see below).

In the no-damping limit $\kappa_s \to 0$, Eq. (7) reduces to the ideal expression

$$N_{\text{sig}}(t) = \left[1 + |\alpha|^2 + 2|\alpha|\cos(\Phi_N)\right] \sinh^2(|g_{\text{eff}}|t), \tag{10}$$

and the coherence function simplifies accordingly. The damping term $e^{-\kappa_s t}$ in Eq. (7) limits the long-time growth of the signal photon number, producing saturation visible in Fig. 2, and reflects the finite lifetime of detector excitations in a dissipative quantum field theory.

This behavior provides a precise optical analog of an Unruh–DeWitt detector coupled to an open environment, where signal loss corresponds to decoherence or detector inefficiency. In contrast, the second-order correlation function $g^{(2)}(0;t)$ probes biphoton coherence between spatially separated detectors. Its sensitivity to the global phase Φ and the fidelity F reveals a transition from separable to entangled signal-mode output, governed by quantum interference and the conditional distinguishability of the idler seed fields.

Our ENBS-based simulator thus realizes a tunable photonic platform for probing entanglement harvesting in relativistic settings. The interplay of phase, gain, fidelity, and damping provides an experimentally accessible connection between nonlinear optical control and quantum-field detector dynamics.

III. SIMULATED VACUUM CORRELATIONS AND ENTANGLEMENT SIGNATURES

In the low-gain regime where $N_{\rm sig}(t) \sim 1$ [29, 30], the ENBS generates time-frequency entangled photon pairs, representing the optical analog of the single-excitation sector in relativistic detector-field models [13]. This regime captures the essence of UDW-type interactions, where detectors interact with the vacuum field without undergoing strong excitations. The phase-resolved control over the biphoton output enables optical simulation of a wide range of relativistic quantum phenomena.

This section investigates how the ENBS reproduces key aspects of detector–field interactions: local stimulated excitation dynamics (Subsec. A), nonlocal quantum interference and correlations (Subsec. B), and the emergence of quantum information signatures such as entanglement and coherence structure (Subsec. C). Together, these results establish a direct analog mapping between relativistic entanglement harvesting and biphoton correlations in the ENBS framework.

A. Stimulated Excitation and Local Detector Analogy

In the UDW model, detector excitation results from interaction with quantum vacuum fluctuations. In the ENBS platform, this excitation is simulated by the spontaneous and stimulated emission of signal photons, governed by the nonlinear interaction between the pump and the seeded idler modes. The signal photon number $N_{\text{sig}}(t)$, as given in Eq. (10), contains three key contributions: spontaneous biphoton generation from vacuum fluctua-

tions, coherent amplification from the idler seed, and phase-dependent interference controlled by the local phase Φ_N . The cosine interference term $2|\alpha|\cos\Phi_N$ reflects coherent control over the gain process, functionally analogous to a time-dependent detector-field coupling in UDW models.

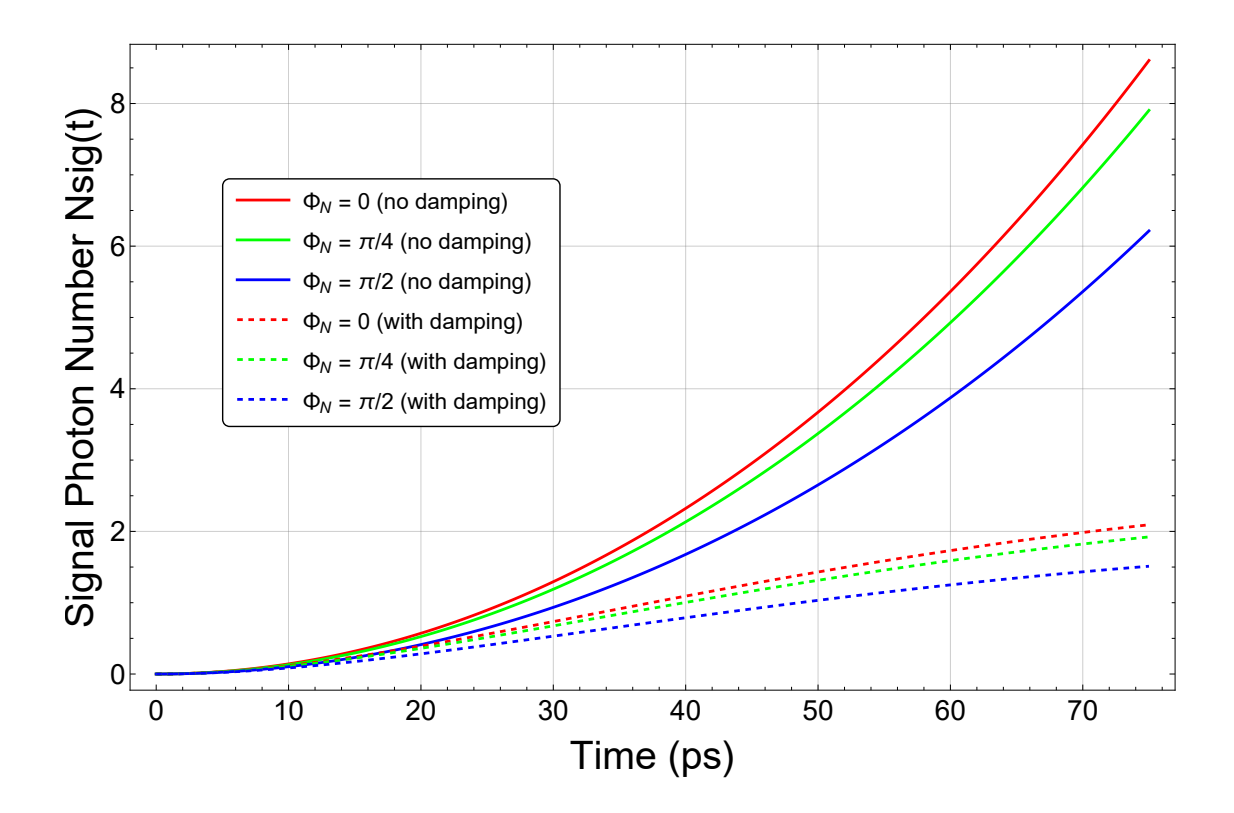


FIG. 2. Signal photon number dynamics with and without damping. The mean photon number $N_{\rm sig}(t)$ is shown for $|\alpha|=5$ and $|g_{\rm eff}|=1$ GHz, comparing the undamped case (solid line) with the damped case (dashed line) for $\kappa_s/(2\pi)=3$ GHz. Saturation occurs within the 75 ps group delay corresponding to a 1-cm PPLN crystal at 807 nm. This illustrates how signal growth is limited by decoherence, analogous to finite-time switching in relativistic detector models. For the asymmetric driving case, see Fig. S1 in the SI.

Figure 2 demonstrates how stimulated signal generation and decoherence interplay within the ENBS simulator. The exponential rise of $N_{\text{sig}}(t)$ under coherent seeding reflects pair production driven by parametric gain. Damping (e.g., from optical losses) leads to saturation, limiting the excitation probability in a way analogous to switching off the UDW detector after a finite interaction window. The ENBS thus faithfully captures both amplification and decoherence effects relevant to relativistic quantum field scenarios.

B. Phase-Controlled Correlations and Nonlocality

Beyond local gain dynamics, the ENBS enables direct simulation of field-induced non-locality. The second-order coherence function $g^{(2)}(0;t)$, defined in Eq. (8), probes biphoton interference across the two ENBS outputs. It depends on the global phase $\Phi = \Delta \phi_p - (\Delta \phi_{sd} + \Delta \phi_s)$ in Fig. 1, encoding coherent pathways for two-photon detection events. When $\Phi = \pi/2$, destructive interference suppresses distinguishability and leads to strong bunching. This phenomenon emulates entanglement harvesting in UDW detector pairs, where spatially separated detectors become entangled through vacuum correlations modulated by coupling phases.

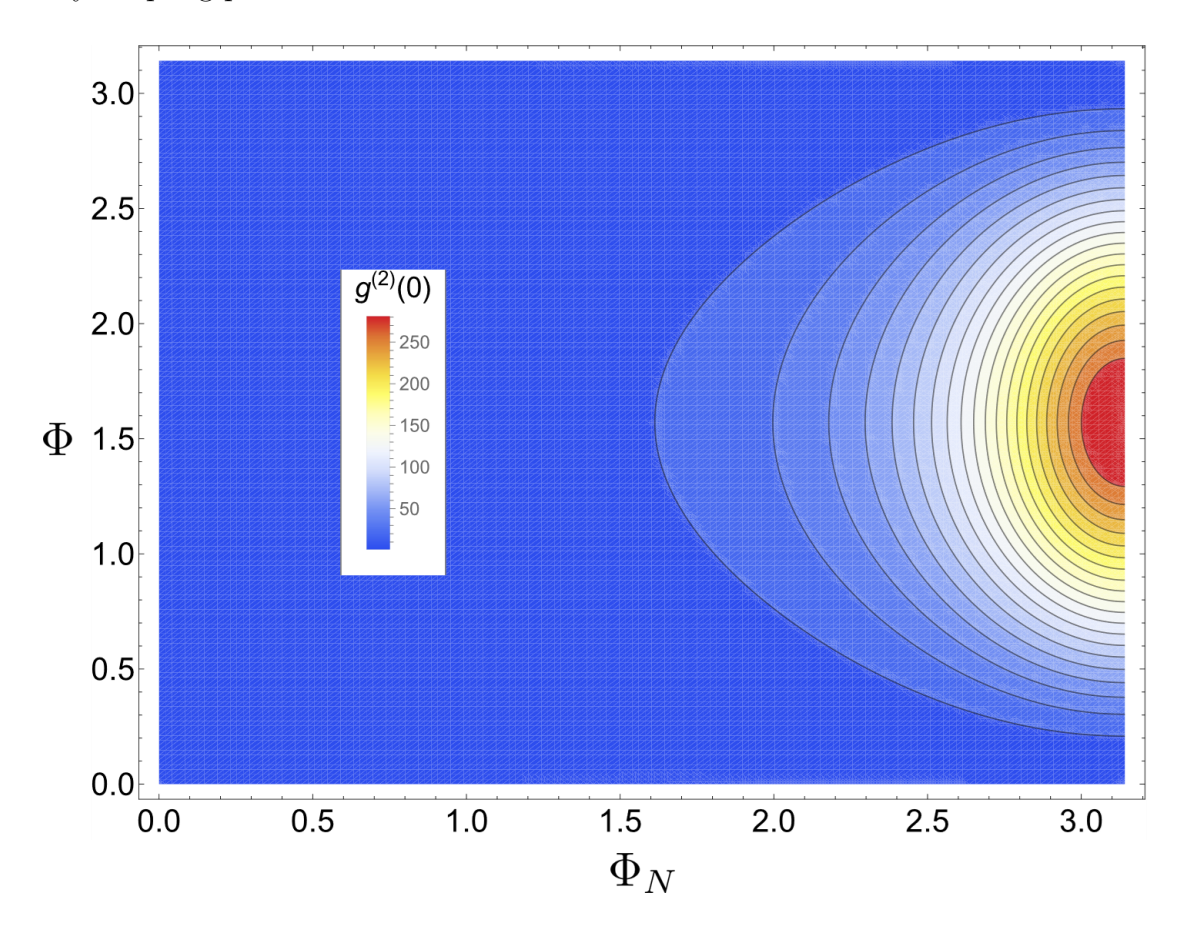


FIG. 3. Contour plot of $g^{(2)}(0; t = 75 \text{ ps})$ as a function of the local phase $\Phi_N = |\Delta \phi_p - \Delta \phi_{sd}|$ and global phase $\Phi = |\Delta \phi_p - (\Delta \phi_s + \Delta \phi_{sd})|$, for $|\alpha| = 2$ and $|g_{\text{eff}}|/(2\pi) = 1$ GHz. Maximal bunching occurs near $(\Phi_N, \Phi) = (\pi, \pi/2)$, revealing the nonlinear interplay between destructive local amplification and enhanced nonlocal quantum correlations.

Figure 3 illustrates the phase landscape of quantum correlations. When $\Phi_N = \pi$, destruc-

tive interference cancels signal generation, but if $\Phi = \pi/2$, strong bunching occurs due to indistinguishability of biphoton emission pathways. Remarkably, even in the regime where $N_{\text{sig}}(t) \to 0$, $g^{(2)}(0;t) \to \infty$, reflecting the enhanced sensitivity of correlation functions to vacuum-induced coherence—an optical signature of field-mediated entanglement.

This counterintuitive behavior demonstrates the core strength of the ENBS as a photonic analog simulator. It separates intensity (local excitation) from correlation (nonlocal coherence), capturing the essence of detector–field entanglement in relativistic quantum field theory.

C. Fidelity, Coherence, and Entanglement of Biphoton States

To quantify the conditional distinguishability of signal-mode outputs in our biphoton simulator, we define the fidelity F as the conditional quantum overlap between the idler branches associated with two coherently seeded ENBSs. Following the formulation in [30], this fidelity is given by

$$F = |\langle \alpha_1, 1 | \langle \alpha_2 | \alpha_1 \rangle | \alpha_2, 1 \rangle|, \qquad (11)$$

where $|\alpha_j, 1\rangle = \hat{a}^{\dagger} |\alpha_j\rangle / \sqrt{1 + |\alpha_j|^2}$ are single-photon-added coherent states (SPACS) [37, 38], and $\langle \alpha_2 | \alpha_1 \rangle = \exp(-|\alpha_1 - \alpha_2|^2/2 + i \operatorname{Im}[\alpha_1^* \alpha_2])$ is the inner product between coherent seed fields.

Evaluating the overlap explicitly (see SI), the fidelity becomes

$$F = \frac{|\alpha_1^* \alpha_2 + 1|}{\sqrt{(1 + |\alpha_1|^2)(1 + |\alpha_2|^2)}} \exp\left(-|\alpha_1 - \alpha_2|^2\right). \tag{12}$$

For symmetric seeding amplitudes $|\alpha_1| = |\alpha_2| = |\alpha|$ and a relative signal-phase difference $\Delta \phi_{\rm sd} \equiv \arg(\alpha_1/\alpha_2)$, we use $\alpha_1 = \alpha e^{i\Delta\phi_{\rm sd}}$, $\alpha_2 = \alpha$, so that

$$F(\Delta\phi_{\rm sd}) = \frac{\left||\alpha|^2 e^{i\Delta\phi_{\rm sd}} + 1\right|}{1 + |\alpha|^2} \exp\left[-2|\alpha|^2 (1 - \cos\Delta\phi_{\rm sd})\right]. \tag{13}$$

This expression shows that F remains a real, non-negative function, with no oscillation in sign but a clear minimum at $\Delta\phi_{\rm sd}=\pi$, where path distinguishability is maximized (Fig. 4). For large $|\alpha|$, the exponential term suppresses phase sensitivity, and $F\to 1$, indicating classical-like coherence. In contrast, for small $|\alpha|$, the fidelity becomes highly sensitive to $\Delta\phi_{\rm sd}$, capturing the quantum interference between entangled biphotons.

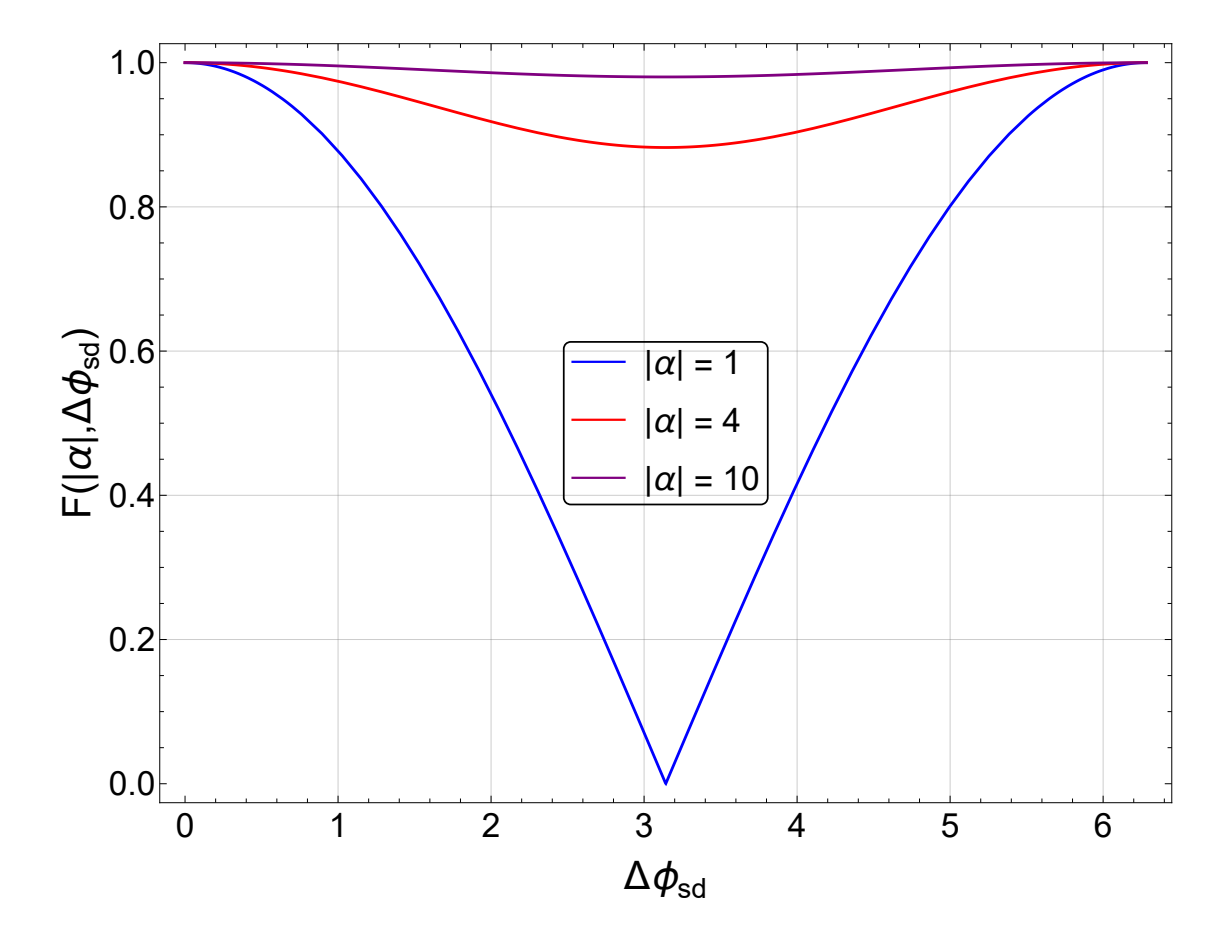


FIG. 4. Fidelity $F(\Delta\phi_{\rm sd})$, defined as the conditional quantum overlap between the idler states $|\alpha_1,1\rangle|\alpha_2\rangle$ and $|\alpha_1\rangle|\alpha_2,1\rangle$, plotted as a function of the relative seeding phase $\Delta\phi_{\rm sd}$ for symmetric amplitudes $|\alpha|=1, 4, 10$. The fidelity reaches a maximum at $\Delta\phi_{\rm sd}=0$ and 2π , and exhibits a minimum at π , where the signal outputs become most entangled due to reduced path indistinguishability. As $|\alpha|$ increases, $F\to 1$ uniformly, reflecting the classical-like coherence of strongly seeded idler states. See Fig. 5 for corresponding visibility and entanglement, and Figs. S2 and S5 for asymmetric cases in the SI.

In the low-gain regime with symmetric seeding, the ENBS signal output approximates a single-photon path-entangled Bell state:

$$|\Psi_{\text{sig}}(t)\rangle \approx \frac{1}{\sqrt{2}} \left(|1\rangle_1 |0\rangle_2 + e^{i\Delta\phi_i} |0\rangle_1 |1\rangle_2 \right),$$
 (14)

with $\Delta \phi_i = \phi_{\alpha,1} - \phi_{\alpha,2}$. The global coherence between SPFC outputs encodes a superposition analogous to detector excitations correlated via a common vacuum field.

We further quantify coherence and quantum correlations [39–41] in the ENBS system using the interference visibility \mathcal{V} , the source (or path) predictability \mathcal{P} , and the entanglement

measure \mathcal{E} , which together satisfy the generalized wave–particle–entanglement complementarity relation established in Refs. [30, 42]:

$$\mathcal{V}^2 + \mathcal{P}^2 + \mathcal{E}^2 = 1. \tag{15}$$

In the symmetric seeding case where $\mathcal{P}=0$, the visibility reaches unity $(\mathcal{V}=1)$, indicating maximal first-order coherence. However, in this regime the entanglement vanishes $(\mathcal{E}=0)$, as the which-path information is fully delocalized and coherence dominates. Conversely, when the signal-mode outputs are path-distinguishable—due to distinguishability of the associated idler states—coherence visibility is suppressed and entanglement is enhanced.

This trade-off is governed by the overlap fidelity defined above. As $|\alpha|$ decreases from large values (e.g., $|\alpha| \sim 10$) toward zero, the idler states transition from nearly parallel to nearly orthogonal $(F \to 0)$, which reduces the coherence $(\mathcal{V} \to 0)$ and increases the entanglement $(\mathcal{E} \to 1)$. This behavior reflects the fundamental quantum resource trade-offs and mirrors UDW detector scenarios in which distinguishability—induced by mismatched coupling phases or switching functions—enhances entanglement harvesting while suppressing coherence.

The relationship between coherence and entanglement can also be seen via the signal-mode source purity [30, 42],

$$\mu_s^2 = \mathcal{P}^2 + \mathcal{V}^2,\tag{16}$$

which bounds the extractable entanglement according to

$$\mathcal{E}^2 = 4\rho_{11}\rho_{22}(1 - F^2) = 1 - \mu_s^2, \tag{17}$$

where ρ_{ij} are the elements of the reduced density matrix in the single-photon signal basis $\{|1,0\rangle_s,|0,1\rangle_s\}$ (see SI). Thus, fidelity $F\sim 1$ implies high purity and low entanglement, while $F\to 0$ corresponds to maximal extractable entanglement. These quantitative relations link phase-controlled optical observables in the ENBS simulator to quantum information measures in relativistic field-theoretic detector models, solidifying the analogy.

D. General Signal-Mode Density Matrix and Quantum Information Measures

To characterize coherence and entanglement in the signal-mode subsystem of the entangled nonlinear biphoton source (ENBS), we begin with the full signal-idler joint state

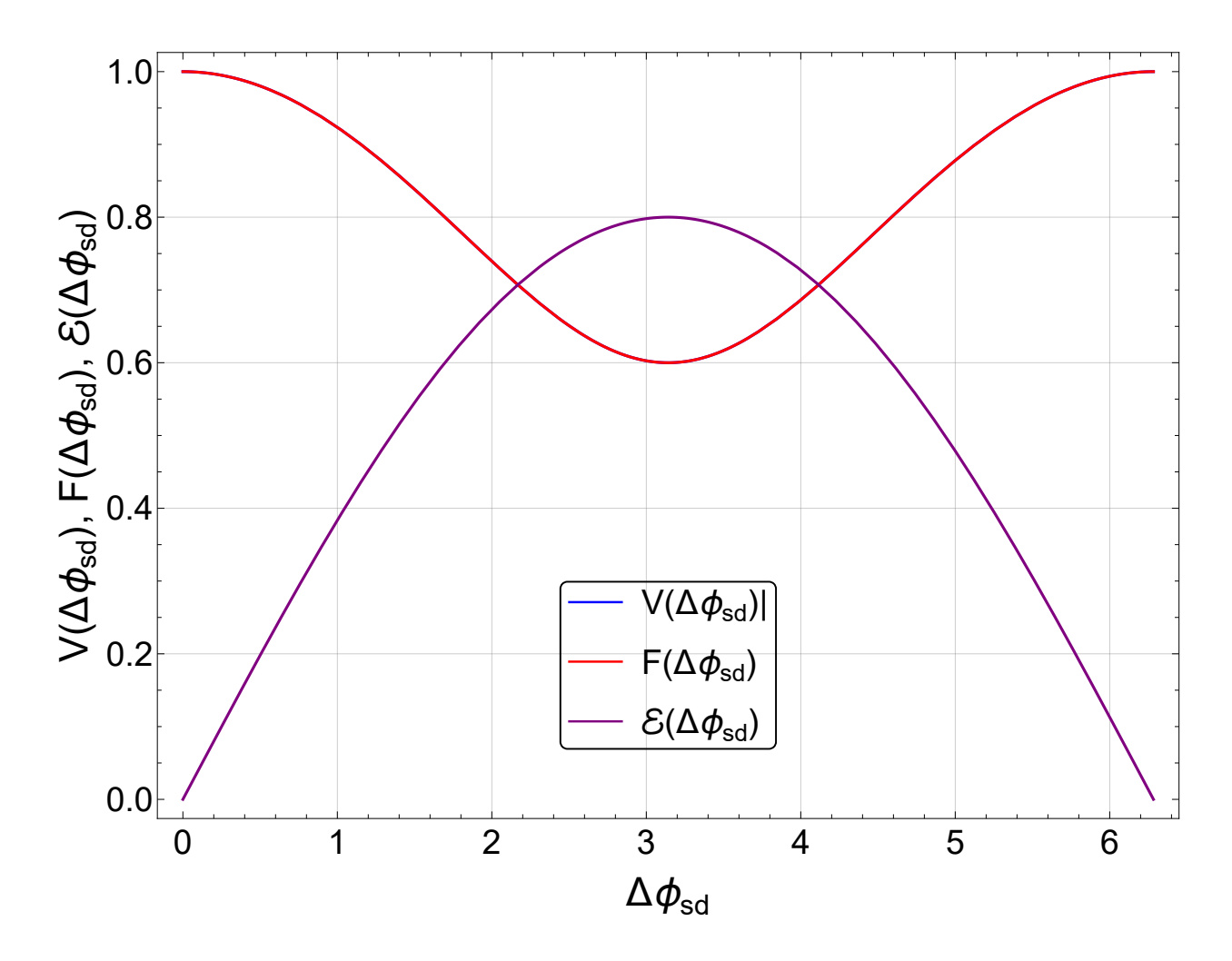


FIG. 5. Plots of fidelity $F(\Delta\phi_{\rm sd})$ (red), visibility $\mathcal{V}(\Delta\phi_{\rm sd})$ (blue), and entanglement $\mathcal{E}(\Delta\phi_{\rm sd})$ (magenta) for symmetric seeding amplitudes $|\alpha_1| = |\alpha_2| = 2$, yielding equal signal-mode populations $\rho_{11} = \rho_{22} = 0.5$. The fidelity and visibility reach their minimum at $\Delta\phi_{\rm sd} = \pi$, where the signal outputs become maximally distinguishable and entanglement is maximized. As $\Delta\phi_{\rm sd} \to 0$ or 2π , $F \to 1$ and $\mathcal{E} \to 0$, indicating high coherence and low entanglement. For asymmetric seeding cases, see Figs. S2–S5 in the SI.

produced by two SPFC sources. The output state is a coherent superposition of two product branches, each consisting of a single-photon-added coherent state (SPACS) in the signal mode and a coherent seed state in the idler mode:

$$|\Psi_{\rm si}\rangle = \frac{1}{\sqrt{\mathcal{N}}} (|\alpha_1, 1\rangle_s \otimes |\alpha_1\rangle_i + |\alpha_2, 1\rangle_s \otimes |\alpha_2\rangle_i),$$
 (18)

where $|\alpha_j, 1\rangle = \hat{a}^{\dagger} |\alpha_j\rangle / \sqrt{1 + |\alpha_j|^2}$ is the single-photon-added coherent state in the signal mode. The corresponding density operator is

$$\hat{\rho}_{\rm si} = |\Psi_{\rm si}\rangle\langle\Psi_{\rm si}|.\tag{19}$$

This coherent superposition ensures the presence of quantum interference between the biphoton branches. Tracing over the idler degrees of freedom yields the reduced signal-mode density matrix, whose coherence and entanglement properties depend sensitively on the overlap between idler coherent states and their SPACS projections.

Tracing over the idler subsystem yields the reduced signal-mode density matrix in the single-photon basis $\{|1,0\rangle, |0,1\rangle\}$ (see SI):

$$\hat{\rho}_{\text{sig}} = \begin{pmatrix} \rho_{11} & \rho_{12} \\ \rho_{12}^* & \rho_{22} \end{pmatrix}, \tag{20}$$

with diagonal terms

$$\rho_{jj} = \frac{1 + |\alpha_j|^2}{2 + |\alpha_1|^2 + |\alpha_2|^2}, \quad j \in \{1, 2\}, \tag{21}$$

and off-diagonal coherence given by

$$|\rho_{12}| = \frac{\sqrt{(1+|\alpha_1|^2)(1+|\alpha_2|^2)}}{2+|\alpha_1|^2+|\alpha_2|^2} \cdot F,$$
(22)

where the conditional fidelity F is defined by the overlap between the idler seed states and their SPACS projections:

$$F = |\langle \alpha_1, 1 | \langle \alpha_2 | \alpha_1 \rangle | \alpha_2, 1 \rangle|$$

$$= \frac{|\alpha_1^* \alpha_2 + 1|}{\sqrt{(1 + |\alpha_1|^2)(1 + |\alpha_2|^2)}} \cdot \exp\left(-|\alpha_1 - \alpha_2|^2\right). \tag{23}$$

In terms of these matrix elements, the first-order coherence visibility is

$$\mathcal{V} = 2|\rho_{12}| = 2F\sqrt{\rho_{11}\rho_{22}},\tag{24}$$

which reduces to $\mathcal{V} = F$ in the symmetric seeding case $|\alpha_1| = |\alpha_2|$, consistent with Subsection III C and Fig. 5.

Experimentally, this first-order coherence visibility \mathcal{V} is obtained from the phase-dependent modulation of the single-photon detection rate $R(\Delta\phi_{\rm sd})$ at the output of the combining beam splitter [see Eq. (5) and Fig. 1], directly linking the reduced density-matrix formalism to the interference measurements in Refs. [29, 30].

The signal source purity of the reduced signal state is

$$\mu_s^2 = \text{Tr}(\rho_{\text{sig}}^2) = \rho_{11}^2 + \rho_{22}^2 + 2\rho_{11}\rho_{22}F^2,$$
 (25)

and the entanglement measure \mathcal{E} , following Ref. [30], is defined via the complementarity relation:

$$\mathcal{E}^2 = 1 - \mu_s^2. \tag{26}$$

Substituting Eq. (25), we obtain:

$$\mathcal{E}^2 = 4\rho_{11}\rho_{22}(1 - F^2),\tag{27}$$

where we used the identity $\rho_{11}^2 + \rho_{22}^2 = 1 - 2\rho_{11}\rho_{22}$. This confirms that the entanglement measure defined via purity is equivalent to that obtained directly from matrix elements, demonstrating internal consistency with Subsection III C.

In the symmetric case $|\alpha_1| = |\alpha_2| = |\alpha|$, we have $\rho_{11} = \rho_{22} = 1/2$, and the density matrix simplifies to:

$$\rho_{\text{sig}} = \frac{1}{2} \begin{pmatrix} 1 & F \\ F & 1 \end{pmatrix}, \tag{28}$$

$$\mathcal{V} = F, \quad \mu_s^2 = \frac{1 + F^2}{2}, \quad \mathcal{E} = \sqrt{\frac{1 - F^2}{2}}.$$
 (29)

This analysis shows that signal coherence visibility \mathcal{V} , purity μ_s^2 , and entanglement \mathcal{E} are determined by the signal-mode populations and the conditional fidelity F, which encodes the distinguishability of the idler pathways. The ENBS platform thus provides a tunable simulator of wave–particle–entanglement complementarity, directly connecting optical phase control to quantum information observables relevant to relativistic field detector dynamics.

IV. CONCLUSION AND OUTLOOK

In summary, the entangled nonlinear biphoton source (ENBS) framework provides a versatile and experimentally accessible platform for simulating the dynamics of relativistic quantum field detectors. By mapping the excitation and coherence properties of coherently seeded single-photon frequency-comb (SPFC) systems onto the Unruh–DeWitt (UDW) detector model, ENBS enables direct photonic analogs of key phenomena such as vacuum-induced

excitation, entanglement harvesting, and phase-sensitive detector responses. Through a combination of analytical modeling and numerical simulation, we have shown that essential features of quantum field theory in curved spacetime—traditionally considered out of experimental reach—can be emulated in a compact quantum optics setting.

Importantly, we have demonstrated that the signal-mode output of the ENBS carries tunable quantum information content, controllable through the relative phase and amplitude of coherent seeding fields. Our analysis of the fidelity, interference visibility, and entanglement entropy of the reduced signal-mode density matrix reveals full phase-dependent control over coherence and entanglement generation. These results, summarized in Figs. 4 and 5, establish ENBS not only as a simulator of detector—field dynamics but also as a programmable quantum light source with engineered coherence properties.

We acknowledge that our simulator employs a single effective idler mode and does not reproduce the full continuum of relativistic quantum fields. In field theory, detector responses arise from two-point vacuum correlators, which are distributional and constrained by the underlying spacetime geometry. While our optical system lacks an infinite-mode field structure, it emulates the detector's local response through engineered temporal correlations mediated by broadband optical pumping and coherent seeding. The fidelity-based distinguishability, signal gain $N_{\text{sig}}(t)$, first-order interference rate $R(\Delta\phi_{\text{sd}})$, and second-order coherence function $g^{(2)}(0;t)$ together capture key observables of UDW-like dynamics in a controllable quantum optical environment. Extensions to include multimode idler continua could enable more direct simulation of spatially structured vacuum correlations and their causal constraints.

Our current implementation does not explicitly model spatial separation or causal disconnection in spacetime. In the Rindler framework, the Unruh effect emerges from tracing over the causally disconnected region of a field, such as the opposite Rindler wedge. Although our simulator operates in a temporally local setting, the observed mixedness and decoherence in the signal mode originate from conditioning on idler measurements and tracing over inaccessible vacuum degrees of freedom. Future architectures incorporating spatially separated ENBS units or idler field continua offer a promising route to emulate spacelike entanglement harvesting and study relativistic quantum correlations across causal boundaries.

Looking forward, this approach opens a new pathway for controlled experimental studies of relativistic quantum phenomena using accessible photonic tools. Future implementations could extend the ENBS platform to simulate detector networks, time-dependent couplings,

or analog spacetime geometries via dispersion engineering and pump shaping. The ability to observe phase-resolved first- and second-order coherence dynamics, single-photon entanglement, and tunable quantum interference positions ENBS at the intersection of quantum optics, relativistic quantum information, and analog gravity. Its scalability and compatibility with frequency-comb and interferometric technologies offer a promising route toward experimental validation of theoretical predictions from quantum field theory in curved spacetime.

[1] W. G. Unruh, Physical Review D 14, 870 (1976).

- [2] B. S. DeWitt, in *General Relativity: An Einstein Centenary Survey*, edited by S. W. Hawking and W. Israel (Cambridge University Press, 1979) pp. 680–745.
- [3] N. D. Birrell and P. C. W. Davies, *Quantum Fields in Curved Space* (Cambridge University Press, 1982).
- [4] B. Reznik, Foundations of Physics **33**, 167 (2003).
- [5] E. Martín-Martínez, M. Montero, and M. del Rey, Phys. Rev. D 87, 064038 (2013).
- [6] G. Salton, R. B. Mann, and G. Adesso, New Journal of Physics 17, 035001 (2015).
- [7] P. Simidzija and E. Martin-Martinez, Physical Review D 98, 085007 (2018).
- [8] K. K. Ng, R. B. Mann, and E. Martín-Martínez, Phys. Rev. D 98, 125005 (2018).
- [9] J. Hu, L. Feng, Z. Zhang, and C. Chin, Nature Physics 15, 785 (2019).
- [10] J. Foo, S. Onoe, and M. Zych, Phys. Rev. D **102**, 085013 (2020).
- [11] T. R. Perche, J. Polo-Gómez, B. d. S. L. Torres, and E. Martín-Martínez, Phys. Rev. D 109, 045013 (2024).
- [12] J.-L. Xie, C.-J. Zhu, J. Tan, and X. Hao, Frontiers in Physics 12, 10.3389/fphy.2024.1513241 (2025).
- [13] S. Wu, Y. Wang, and W. Liu, arXiv preprint arXiv:2506.14115.
- [14] K. K. Ng, R. B. Mann, and E. Martín-Martínez, Phys. Rev. D 97, 125011 (2018).
- [15] N. Friis, A. R. Lee, K. Truong, C. Sabín, E. Solano, G. Johansson, and I. Fuentes, Physical Review Letters 110, 113602 (2013).
- [16] M. Ahmadi, D. E. Bruschi, C. Sabín, G. Adesso, and I. Fuentes, Scientific Reports 4, 4996 (2014).

- [17] R. H. Jönsson, E. Martín-Martínez, and A. Kempf, Physical Review A 89, 022330 (2015).
- [18] D. E. Bruschi, C. Sabín, P. Kok, G. Johansson, P. Delsing, and I. Fuentes, Scientific Reports 6, 18349 (2016).
- [19] J. Rodríguez-Laguna, L. Tarruell, M. Lewenstein, and A. Celi, Phys. Rev. A 95, 013627 (2017).
- [20] J. Kohlrus, J. Louko, I. Fuentes, and D. E. Bruschi, (2019).
- [21] E. Adjei, K. J. Resch, and A. M. Brańczyk, Phys. Rev. A 102, 033506 (2020).
- [22] T. Sheng, J. Qian, X. Li, Y. Niu, and S. Gong, Phys. Rev. A 103, 013301 (2021).
- [23] R. Lopp and E. Martín-Martínez, Physical Review A 103, 013703 (2021).
- [24] Z. Tian, L. Wu, L. Zhang, J. Jing, and J. Du, Physical Review D 106, L061701 (2022).
- [25] C. Viermann, M. Sparn, N. Liebster, M. Hans, E. Kath, Álvaro Parra-López, M. Tolosa-Simeón, N. Sánchez-Kuntz, T. Haas, H. Strobel, S. Floerchinger, and M. K. Oberthaler, Nature 611, 260 (2022).
- [26] E. P. G. Gale and M. Zych, Physical Review D 107, 056023 (2023).
- [27] H.-T. Zheng, X.-F. Zhou, G.-C. Guo, and Z.-W. Zhou, Physical Review Research 7, 013027 (2025).
- [28] P. A. LeMaitre, T. R. Perche, M. Krumm, and H. J. Briegel, Physical Review Letters 134, 190601 (2025).
- [29] S. K. Lee, N. S. Han, T. H. Yoon, and M. Cho, Communications Physics 1, 51 (2018).
- [30] T. H. Yoon and M. Cho, Science Advances 7, eabi9268 (2021).
- [31] C. M. Wilson, G. Johansson, A. Pourkabirian, M. Simoen, J. R. Johansson, T. Duty, F. Nori, and P. Delsing, Nature 479, 376 (2011).
- [32] V. V. Dodonov, Physics 7, 10 (2025).
- [33] Y. N. Freitag, J. Pinske, and J. Sperling, Entangled quantum trajectories in relativistic systems (2024), arXiv:2410.05995 [quant-ph].
- [34] K. S. Kumar and J. Marto, Universe 10, 320 (2024).
- [35] D. Barman and B. R. Majhi, Annals of Physics 465, 169678 (2024).
- [36] D. Barman and B. R. Majhi, Physics Letters B 868, 139631 (2025).
- [37] G. S. Agarwal and K. Tara, Phys. Rev. A 43, 492 (1991).
- [38] A. Zavatta, S. Viciani, and M. Bellini, Science **306**, 660 (2004).
- [39] T. J. Herzog, P. G. Kwiat, H. Weinfurter, and A. Zeilinger, Physical Review Letters 75, 3034 (1995).

- [40] L. Maccone, D. Bruß, and C. Macchiavello, Physical Review Letters 114, 130401 (2015).
- [41] A. Heuer, R. Menzel, and P. W. Milonni, Physical Review Letters 114, 053601 (2015).
- [42] X.-F. Qian and G. S. Agarwal, Physical Review Research 2, 012031 (2020).

METHODS

The Supplementary Information (SI) provides full and explicit derivations of the theoretical model, including the exact time-dependent expressions for the signal-mode photon number $N_{\text{sig}}(t)$, the second-order coherence function $g^{(2)}(0;t)$, and the reduced density matrix formalism used to quantify fidelity, coherence visibility, and entanglement. These results incorporate both symmetric and asymmetric coherent seeding conditions and include the effects of signal-mode damping via Lindblad evolution.

In this Methods section, we describe the core design principles and experimental parameters of the proposed quantum optical simulator based on ENBS. We also summarize the essential theoretical ingredients and approximations necessary to interpret the main observables and simulate UDW detector dynamics in a tunable, photonic platform.

In addition to intensity and coincidence measurements, the setup also enables measurement of the single-photon detection rate $R(\Delta\phi_{\rm sd})$ at one output of the combining beam splitter. This quantity exhibits sinusoidal modulation with the seeding-phase difference $\Delta\phi_{\rm sd}$, providing direct access to the first-order (single-photon) coherence visibility of the signal field, as demonstrated in Refs. [29, 30].

Quantum optical simulator design

Our analog quantum simulator is based on two coherently seeded SPFC sources implemented via type-0 spontaneous parametric down-conversion (SPDC) in PPLN waveguides. Each SPFC is pumped by a narrowband optical frequency comb centered at 530 nm, and seeded by a continuous-wave coherent idler field at 1542 nm. The output consists of entangled signal-idler photon pairs distributed across frequency bins. The pump and seed phases are independently controlled by phase modulators to implement local and global phase mismatches Φ_N and Φ , as defined in Eqs. (4a)-(4b) of the main text.

Effective Hamiltonian and master equation

The effective system Hamiltonian is

$$\hat{H}_{\text{ENBS}} = \hbar |g_{\text{eff}}| \sum_{j=1}^{2} \left(e^{i\phi_{p,j}} \hat{A}_{\text{SM},j}^{\dagger} \hat{a}_{i,j}^{\dagger} + e^{-i\phi_{p,j}} \hat{A}_{\text{SM},j} \hat{a}_{i,j} \right), \tag{30}$$

where $\hat{A}_{\text{SM},j}$ denotes the signal supermode operator, $\hat{a}_{i,j}$ the annihilation operator for the j-th idler mode, and $\phi_{p,j}$ is the j-th pump phase. The nonlinear interaction strength $|g_{\text{eff}}|$ is calibrated from the measured SPDC gain in the undepleted pump regime. The evolution of the system density matrix $\hat{\rho}(t)$ includes optical loss and is governed by the Lindblad master equation:

$$\frac{d\hat{\rho}}{dt} = -\frac{i}{\hbar} [\hat{H}_{\text{ENBS}}, \hat{\rho}] + \sum_{j=1}^{2} \left[\mathcal{D}[\sqrt{\kappa_s} \hat{A}_{\text{SM},j}] + \mathcal{D}[\sqrt{\kappa_i} \hat{a}_{i,j}] \right] \hat{\rho}, \tag{31}$$

with decay rates κ_s and κ_i corresponding to signal and idler losses. The superoperator $\mathcal{D}[\hat{L}]\hat{\rho} = \hat{L}\hat{\rho}\hat{L}^{\dagger} - \frac{1}{2}\{\hat{L}^{\dagger}\hat{L},\hat{\rho}\}$ models decoherence via photon loss of our ENBS system in Fig. 1.

Analytical solutions and numerical validation

We derive closed-form analytical solutions for the signal photon number $N_{\text{sig}}(t)$ and normalized second-order coherence $g^{(2)}(0;t)$ under coherent seeding, using both Heisenberg-Langevin equations and perturbative methods. In the low-gain limit, the signal state is approximated by a single-photon superposition, enabling derivation of entanglement, coherence visibility, and predictability as in Ref. [30]. In the high-gain regime, time-resolved correlation functions are obtained numerically by solving the Lindblad equation using truncated Fock-space representations.

Simulation parameters and physical constraints

All simulation parameters are chosen to match experimentally feasible values. For Figs. 2 and 3, the nonlinear gain rate is set to $|g_{\text{eff}}|/(2\pi) = 10 \text{ GHz}$, with seed amplitude $|\alpha|$ varied

between 1 and 5. Damping rates $\kappa_s/(2\pi) = 2.5$ GHz and $\kappa_i \ll \kappa_s$ account for signal loss within the 1-cm PPLN interaction length, corresponding to a group delay of approximately 75 ps. These values are consistent with state-of-the-art integrated SPDC platforms.

Quantum information characterization

We characterize the quantum information properties of the ENBS output via the reduced signal-mode density matrix ρ_s , obtained by tracing out the idler degrees of freedom. The coherence visibility \mathcal{V} , predictability \mathcal{P} , and entanglement measure \mathcal{E} satisfy the wave–particle–entanglement identity [30, 42]:

$$\mathcal{V}^2 + \mathcal{P}^2 + \mathcal{E}^2 = 1. \tag{32}$$

The fidelity F between conditional idler states determines entanglement via $\mathcal{E}^2 = 2\rho_{11}\rho_{22}(1 - F^2)$, with ρ_{ij} the signal-mode density matrix elements in the $\{|1,0\rangle_s, |0,1\rangle_s\}$ basis. This enables direct interpretation of phase-resolved measurements in terms of quantum field-detector analogs.

Data availability The data that support the findings of this study are available from the corresponding author upon reasonable request.

Code availability The codes used for analysis of all figures are available from the corresponding author upon reasonable request.

Acknowledgements T. H. Yoon acknowledges Alexander Rothkopf for reading the manuscript and providing helpful comments, as well as Sun Kyung Lee and Mincheng Cho for their extended collaboration on SPFC state generation and its applications in the ENBS system. This work was supported by the National Research Foundation of Korea under Grant No. NRF-2022M3K4A1094781.

Author contributions T. H. Yoon conceived the research idea, developed the theoretical framework, performed all analytical derivations and numerical simulations, and wrote the manuscript.

Competing interests The authors declare no competing interests.